SAND REPORT
SAND2002-3963
Unlimited Release
Printed December 2002

Nanostructured Materials Integrated in Microfabricated Optical Devices

Darryl Y. Sasaki, Shanalyn A. Kemme, C. Jeffrey Brinker, Mial E. Warren, Michael B. Sinclair, Julie A. Last, Bruce Bondurant, Tina A. Waggoner, Joel R. Wendt, Tony Carter, Sally Samora, Yi Yang

Prepared by
Sandia National Laboratories
Albuquerque, New Mexico 87185 and Livermore, California 94550

Sandia is a multiprogram laboratory operated by Sandia Corporation, a Lockheed Martin Company, for the United States Department of Energy under Contract DE-AC04-94AL85000.

Sandia National Laboratories

Issued by Sandia National Laboratories, operated for the United States Department of Energy by Sandia Corporation.

Available to DOE and DOE contractors from
U.S. Department of Energy
Office of Scientific and Technical Information
P.O. Box 62
Oak Ridge, TN 37831

Telephone: (865)576-8401
Facsimile: (865)576-5728
E-Mail: reports@adonis.osti.gov
Online ordering: http://www.doe.gov/bridge

Available to the public from
U.S. Department of Commerce
National Technical Information Service
5285 Port Royal Rd
Springfield, VA 22161

Telephone: (800)553-6847
Facsimile: (703)605-6900
E-Mail: orders@ntis.fedworld.gov
Online order: http://www.ntis.gov/help/ordermethods.asp?loc=7-4-0#online

SAND 2002-3963
Unlimited Release
Printed December 2002

Nanostructured Materials Integrated in Microfabricated Optical Devices

Darryl Y. Sasaki. Julie A. Last, Bruce Bondurant, Tina A. Waggoner
Biomolecular Materials and Interfaces Department

C. Jeffrey Brinker
Chemical Synthesis and Nanomaterials Department

Shanalyn A. Kemme, Joel R. Wendt, Tony Carter, Sally Samora
Photonics Microsystems Technology Department

Mial E. Warren
Microsystems Partnerships Department

Michael B. Sinclair
Microsystems Materials, Tribology and Technology Department

Sandia National Laboratories
P.O. Box 5800
Albuquerque, New Mexico, 87185-1413

Yi Yang
University of New Mexico
Department of Chemical and Nuclear Engineering
Albuquerque, New Mexico 87106

Abstract

This project combined nanocomposite materials with microfabricated optical device structures for the development of microsensor arrays. For the nanocomposite materials we have designed, developed, and characterized self-assembling, organic/inorganic hybrid optical sensor materials that offer highly selective, sensitive, and reversible sensing capability with unique hierarchical nanoarchitecture. Lipid bilayers and micellar polydiacetylene provided selective optical response towards metal ions (Pb(II), Hg(II)), a lectin protein (Concanavalin A), temperature, and organic solvent vapor. These materials formed as composites in silica sol-gels to impart physical protection of the self-assembled structures, provide a means for thin film surface coatings, and allow facile transport of analytes. The microoptical devices were designed and prepared with two- and four-level diffraction gratings coupled with conformal gold coatings on fused silica. The structure created a number of light reflections that illuminated multiple spots along the silica surface. These points of illumination would act as the excitation light for the fluorescence response of the sensor materials. Finally, we demonstrate an integrated device using the two-level diffraction grating coupled with the polydiacetylene/silica material.

Acknowledgment

Sandia is a multiprogram laboratory operated by Sandia Corporation, a Lockheed Martin Company, for the United States Department of Energy under Contract DE-AC04-94AL85000.

Contents

Figures

Introduction

Materials, by their nature, are stable and inert substances typically insensitive to their environment. Some types of materials do have certain innate selective absorption of chemicals that can change the materials physical properties (e.g., swelling, viscosity), such as those used in sensor films. However, the selectivity and response of these materials are difficult to predict and, thus, tailor to specific analytes of interest. Furthermore, the response times are typically slow due to lengthy equilibration times from the slow molecular dynamics and they are incompatible with biological materials. Due to these poor characteristics interest in creating so-called "smart" materials having specific response/function to chemical or physical stimuli has grown in recent years.

We have developed a new class of materials that are a composite of a highly ordered inorganic matrix entrained with self-assembled organic structures functionalized with molecular receptors that can yield rapid, selective, and sensitive optical response to chemical, biological, and physical stimuli. These material's structure and function are a result from the design of the molecular and supramolecular structures and we thus refer to them as nanocomposites. Self-assembly of the organic components dictate the formation of the inorganic structure and in turn the inorganic matrix can influence the organic material's response, stability, and signal transduction. In addition to the development of these composites as sensor materials, we also integrated them into microfabricated structures for the development of unique optical devices with tunable properties. By forming the material as the optical device we may create new possibilities such as chemically tunable lattices or optical switches and waveguides. Microfabrication of these optical devices could provide a unique capability in preparing inexpensive sensor array platforms for combinatorial molecular and materials discovery routes or even totally new photonic structures.

To achieve a rapid, tunable, and reversible optical response we used functionalized, molecularly dynamic self-assembled organic materials. Molecular reorganization in the material, induced by chemical recognition or other selective physical stimulation, is transduced into a optical change that can be detected as a fluorescence or colorimetric response. We have employed the unique color change properties of polydiacetylene materials and fluorescence response of labeled lipid bilayers. With these materials response times can be on the order of seconds with complete reversibility. The lipid bilayer mimics the cell membrane making it an ideal material for molecular recognition of biospecies, in particular biological warfare agents, which typically target the cell membrane. The selectivity of these materials for metal ions and proteins can be readily tailored by replacing the recognition groups at the material's surface.

The self-assembled organic structures were then incorporated into inorganic materials via the sol-gel technique. In situ techniques were used to allow the facile formation of the composite material with added advantages of full incorporation throughout the matrix and intimate association between the organic and inorganic components.

We will also demonstrate the integration of the nanocomposite material with an microoptical substrate containing diffractive optics. The optical substrate has three roles: mechanical support of the sensing film, spatial discrimination of the sensing films for combinatorial sensing, and spatial distribution of the optical signals. The diffractive optics collects, collimates, and redirects the excitation beam to appropriate sensing film patches. The approach is relatively simple and with low optical loss.

Results and Discussion

Self-assembled optical sensor materials

Metal ion sensing lipid bilayers

Synthetically prepared lipids, functionalized at the headgroup position with chemical receptors and at the tail position with a fluorescent probe, are incorporated into phospholipid bilayers to form the sensor materials. Binding of specific ligands from solution induces a change in the aggregational state of the receptors, resulting in a change in fluorescence of the bilayers. Depending on the ligand of interest, it is possible to induce the receptor lipids to either aggregate or disperse in response to the chemical recognition event. In the case of metal ions, the receptors initially are in the aggregated state, caused by the phase separation of the liquid-phase receptor-lipids from solid-phase matrix lipids (e.g., distearylphosphatidyl choline (DSPC)). Binding of metal ions activates the receptor-lipids and causes them to disperse into the DSPC matrix.

We have designed and prepared a lipid membrane that was functionalized with a receptor that would be minimally affected by solution conditions (e.g., pH, salt concentration), large enough to be detectable by atomic force microscopy (AFM) in small aggregates, simple in functionality to allow a straightforward analysis, and sufficiently polar to serve as a lipid headgroup. A functional group that accommodates all of these characteristics is the crown ether. The 18-crown-6 group, in particular, should not only offer excellent properties as the lipid headgroup but may provide a material with selective affinity, and thus sensing capability, for toxic metal ions of interest such as Pb^{2+} or Hg^{2+}.[1,2] The resulting functionalized bilayer allowed us to gain some insight into the mechanism of the chemical recognition-induced receptor aggregation and the macro- to nano-scale changes of receptor assemblies in the two-dimensional space of the lipid membrane. Several techniques used in this study allowed us to probe the molecular to supramolecular interactions within the bilayer. NMR studies were used

AFM imaging provided the means to observe nanoscale structures as they responded to ligand binding.

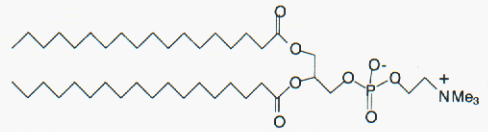

DSPC

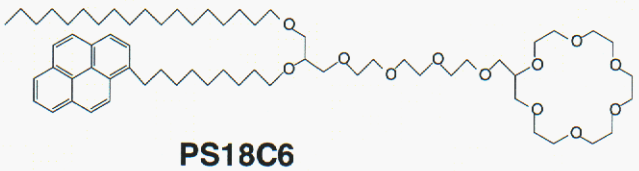

PS18C6

Figure 1. Molecular structures of distearylphosphatidylcholine (DSPC) and pyrene-labeled, 18-crown-6 functionalized lipid (PS18C6).

The crown ether functionalized lipid, PS18C6, was prepared by coupling 8[1-octadecyl-2-(9-(1-pyrene)nonyl)-*rac*-glyceroyl]-3,6-dioxaoctan-1-ol (PSOH),[3] with 2-(hydroxymethyl)-18-crown-6 (Figure 1). Coupling of these two components was facilitated by mesylation of the PSOH lipid followed by reaction with 2-(hydroxymethyl)-18-crown-6 in a DMSO solution with KOH, at 85 °C. The product lipid, PS18C6, was isolated by flash chromatography as a light green, viscous oil. All spectral data corresponded with the proposed structure. Small unilamellar vesicles (SUV) of 5 mole % of PS18C6 in a DSPC membrane were prepared in a MOPS buffer solution via ultrasonication. The vesicle sizes ranged from 80 – 120 nm in diameter, as determined by transmission electron microscopy (TEM).

Vesicles of the 5% PS18C6/DSPC bilayers were irradiated at 346 nm, producing a fluorescence spectrum with emission from both pyrene monomer (λ_{max}^{em} = 376 nm) and excimer (λ_{max}^{em} = 464 nm) (Figure 2). The intensity ratio of the excimer (E) to monomer (M) was typical of a pyrene-labeled lipid with a hydrophilic headgroup (e.g., dithioamide, alcohol).[4,5] Bilayers prepared in buffered saline solution exhibited relatively constant E/M values over a pH range of 4 – 9, indicating stability of the bilayers to pH. In contrast, similar studies performed with bilayers prepared with 5 mole % of the iminodiacetic acid-functionalized lipid PSIDA[6] exhibited a large variance in normalized E/M value with pH, changing from 0.39 at pH 4 to 1.0 at pH 7.5.[5]

The 5% PS18C6/DSPC vesicles responded selectively to the presence of lead and mercuric ions with a change in excimer to monomer intensities from the pyrene fluorophore. An example of the optical response is shown in Figure 3, where $Pb(NO_3)_2$ was present at varying concentrations in the vesicle solution. As the lead concentration was increased, the excimer emission decreased with a

concomitant increase in the monomer emission. Numerous other metal ions were sampled but no optical response was observed. Those sampled were $NiCl_2$, $SrCl_2$, $CrCl_3$, $CaCl_2$, $CeCl_3$, $CsCl_2$, $CoCl_2$, and $MnCl_2$ at concentrations up to 0.5 mM, AgCl and $CdCl_2$ up to 1.0 mM, $CuCl_2$ up to 0.1 mM, and KCl and RbCl up to 100 mM. Due to solubility issues, $Pb(NO_3)_2$ was used in preference to $PbCl_2$ and $Pb(Ac)_2$. The latter two salts had poor solubility in MOPS buffer solution at the higher concentrations (>100 μM). At lower concentrations, however, the responses of the different lead salts were virtually identical.

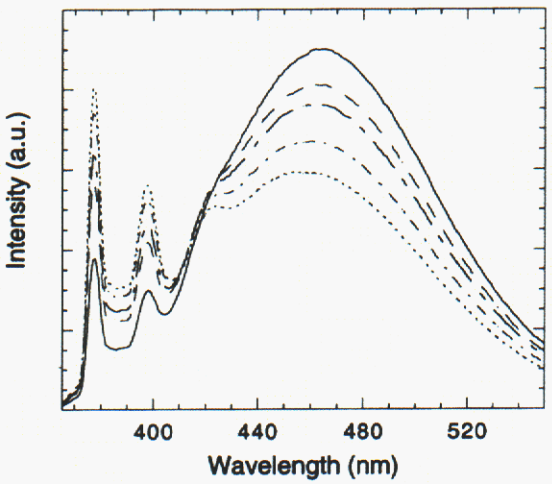

Figure 2. Fluorescence spectra of 5% PS18C6/DSPC liposomes (λ_{ex} = 346 nm) in MOPS buffer solution (pH 7.4) in the absence (——) and presence of $Pb(NO_3)_2$ at 1μM (– –), 10 μM (— -), 100 μM (– -), and1.0 mM (- -).

Figure 3 shows a plot of the normalized E/M fluorescence of the 5% PS18C6/DSPC vesicles as they responded to increasing metal ion concentration in solution. The data show that the bilayer yielded a fairly linear response to Pb(II) from 10^{-7} to 10^{-4} M. At concentrations greater than 10^{-4} M, the response exceeded the linear response defined by the lower concentrations. The response for the mercuric ion was less pronounced but just as sensitive as the Pb(II) response. Sensitivities for Pb(II) and Hg(II) were at the sub-micromolar level (i.e., low-ppb sensitivity). The lipid bilayers could also be regenerated to their original optical state through the addition of EDTA to the solution.

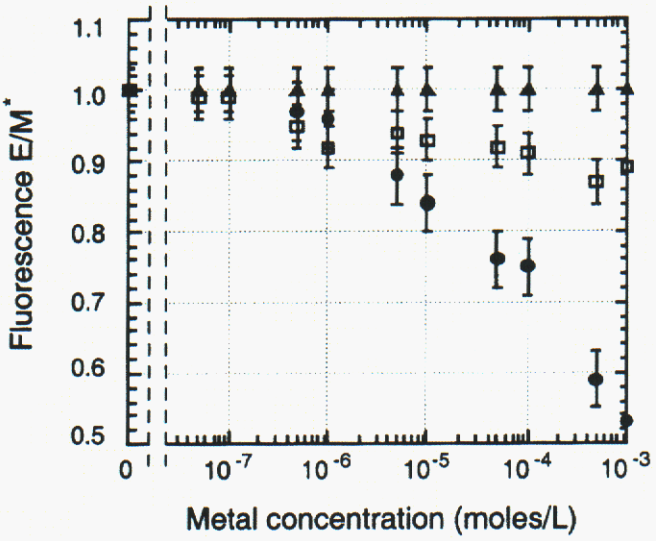

Figure 3. Normalized (*) E/M fluorescence data for 5% PS18C6/DPSC liposomes responding to a logarithmic increase of $Pb(NO_3)_2$ (●), $HgCl_2$ (□), and numerous metal salts listed in the text, which include $CuCl_2$, $NiCl_2$, $CdCl_2$, $CoCl_2$, $CaCl_2$, $CsCl_2$, and $SrCl_2$ (▲).

Previous studies with metal ion sensitive lipid bilayers[6] found that the E/M changes observed upon metal ion addition were a reflection of the change in the aggregational state of the lipids upon chemical recognition. The pyrene-labeled lipid, which has a T_c (crystalline-to-liquid crystalline phase transition temperature) well below room temperature, and the DSPC matrix with a T_c of 55 °C, phase separate resulting in the aggregation of PS18C6 lipids and a high local concentration of pyrene moieties in the two-dimensional space of the lipid bilayer. The high pyrene concentration thus promotes excimer formation. This lipid aggregation is, however, dependent upon the physical state of the lipid. Initially, a charge neutral receptor-lipid would have its distribution within the membrane dictated by the crystalline domain formation of the DSPC lipids. Changing the physical characteristics of the lipid, such as the addition of electrostatic charge from metal ion chelation, can introduce repulsive forces that override the phase separation of the lipid components. This repulsion will then result in the dispersion of the receptor-lipids (Figure 4).

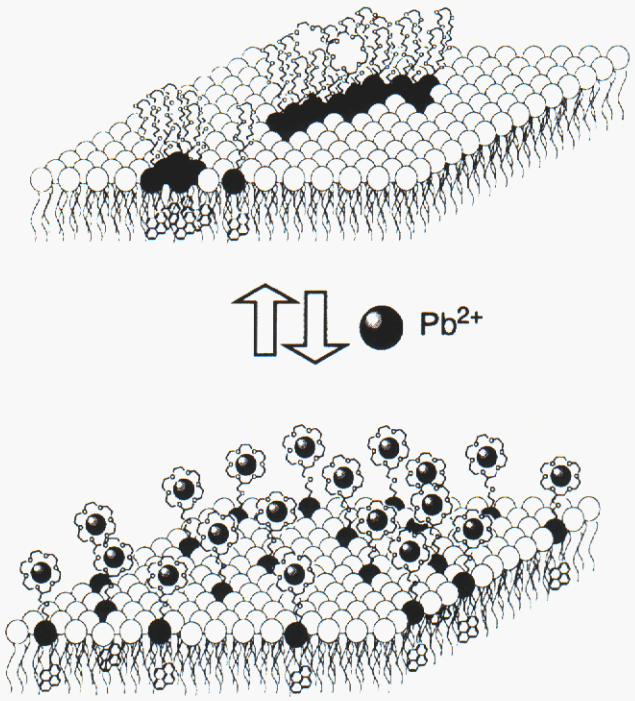

Figure 4. Schematic of one leaflet of a PS18C6 (darkened headgroup)/DSPC mixed lipid membrane before (above) and after (below) addition of Pb^{2+} ion. Recognition of Pb^{2+} by the crown ether causes the lipid's headgroup to become cationic resulting in electrostatic repulsion between other Pb^{2+}-bound lipids.

Visualization of sub-microscopic changes in lipid aggregation was accomplished with AFM imaging of the lipid bilayers supported on a mica surface. A 20% PS18C6/DSPC bilayer was formed on the mica surface via the vesicle fusion technique in an AFM solution cell. The 20% PS18C6/DSPC composition provided the most distinct AFM images, compared to lower mole ratios of 5 and 10%.[7] The bilayer coverage was fairly homogeneous over the mica with holes of micron size or smaller sparsely distributed in the film. These holes provided a reference to measure film thickness, which was approximately 54 ± 3Å, consistent with a DSPC bilayer (~47Å) supported upon an 8 - 10Å water layer. Figure 9A shows a typical 1.8 μm x 1.8 μm AFM image of the bilayer. The area was free of holes but populated with dark and light regions. The height difference between the dark and light regions was 8 ± 1 Å,[8] which is approximately the height difference between DSPC and PS18C6, as determined by a simple space-filling model. Furthermore, using a pixel counting analysis we found that the light regions in the membrane accounted for roughly 20% of the surface, coincident with the loading of the crown ether lipid in the DSPC matrix. From these pieces of data we could assign the dark regions to the DSPC matrix and the light regions as areas rich in PS18C6.

Nanoscale features of Figure 5 A-D changed in size and intensity as the membrane responded to the introduction or removal of Pb(II) to the solution. The images were taken from the

same area over the course of the experiment (total experimental time < 20 minutes). The structures in the membrane are composed of sub-micron scale islands and 10 – 30 nm wide filaments of PS18C6-rich regions. The widths of those filaments are roughly equivalent to one to two dozen PS18C6 molecules. Addition of $Pb(NO_3)_2$ (100 μM) causes those structures to diminish in size and intensity and causes significant restructuring of the membrane (Figure 5B). Removal of the Pb(II) ion from the membrane surface, by the addition of a solution of 100 μM EDTA, induces a rapid reaggregation of the PS18C6 lipids that is readily perceptible by the increase in size and intensity of the light regions (Figure 5C). And finally, reexposing the membrane to a 100 μM solution of $Pb(NO_3)_2$ reverts the nanoscale features again to reduced dimensions (Figure 5D). These chemical recognition-induced membrane reorganization events occur on a time scale faster than that needed to inject the solutions and image the material (< 1 minute). If the fluorescence data can be used as an indicator of the rate at which the reorganization occurs, then the time scale is actually on the order of seconds. It should be noted that the AFM images themselves are stable over the course of hours. As a control, when Ca(II) and Mn(II) was used in place of Pb(II) no change in the nanoscale structures were seen. This series of experiments demonstrates the reversibility of this molecularly dynamic, chemical recognition driven system.

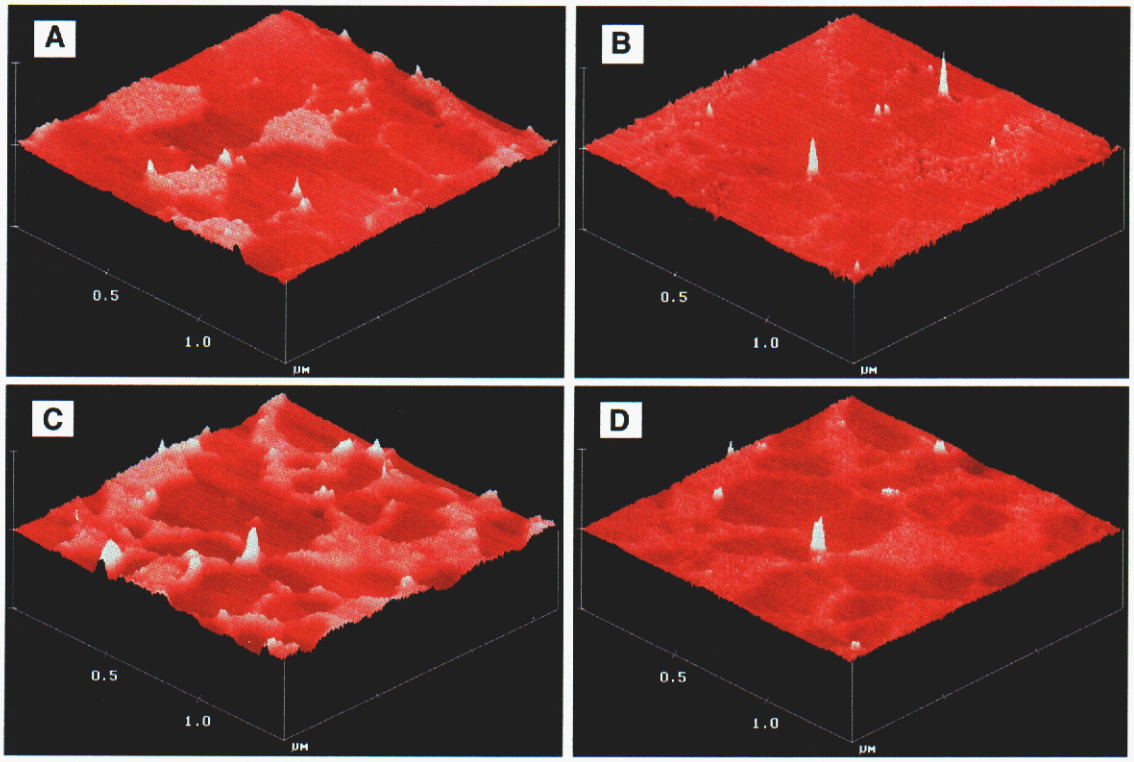

Figure 5. AFM topographic images of a 20% PS18C6/DSPC bilayer supported on a mica surface demonstrating the actuation of the film from aggregated to dispersed states with Pb^{2+} ions. The membrane in the (A) initial state, then (B) after addition of 0.1 mM $Pb(NO_3)_2$, followed by (C) addition of 0.1 mM EDTA, and finally (D) after addition of 0.1 mM $Pb(NO_3)_2$ again. All solutions were aqueous saline (0.1 M NaCl).

The crown ether functionalized lipid bilayer provides a unique platform to demonstrate the rapid, reversible, and selective molecular reorganization of lipid membranes, at both the macro- and nano-scales, induced through chemical recognition at the membrane surface. Furthermore, the distinctive fluorescence response of the bilayer to metal ion binding makes these materials attractive for sensor applications. The selectivity observed for Pb(II) and Hg(II) over Cd(II) and Sr(II), which have comparable binding constants (K_a) in water, suggests that the 18-crown-6 group on the membrane surface resides in a unique medium that allows for different, and sometimes enhanced, discrimination for specific ions. The bilayers also provided a means to demonstrate that the lipid dispersion observed with metal ion presence was due to electrostatic repulsion of the cations formed by the 1:1 binding of metal ions at the receptor headgroup. This molecular reorganization was evident at the nanoscale, by AFM. A combination of spectroscopic and scanning probe studies can be used to generate a comprehensive picture of mixed membrane systems and their changes in organization upon chemical recognition events.

Protein sensing lipid bilayers

Lipid bilayer systems can be used as unique biosensors to detect proteins in solution (e.g., His-tagged proteins,[3] cholera toxin[9]). As a sensor material these functionalized lipid bilayers offer excellent biocompatible properties, reversible affinity and response, and an optical detection scheme intrinsic within the material alleviating the need for protein tagging. It is our expectation that specific chemistries of the lipids, host-guest interactions, and membrane compositions will give rise to unique insights into how cellular membranes react to specific ligands and environmental stimulation. Of particular interest is how membranes respond to adhesion, of which protein-carbohydrate complexation plays a large role.[10] Here, we describe the preparation of a new fluorescently-tagged glycolipid (mannosaminyl headgroup), its incorporation in phosphatidyl-choline lipid bilayers, the selective binding of the lectin Concanavalin A (Con A), and the reorganization of the membrane in response to the binding of the protein. Fluorescence data reveals that the glycolipid disperses at a slow rate within the bilayer upon Con A binding while scanning probe imaging of the surface finds that the protein binds to regions in the bilayer initially rich with the glycolipid.

Pyrene-labeled, carbamate-linked D-mannosamine functionalized lipid, PSMU, was prepared in two steps from PSOH (Figure 6). The headgroup was formed by linking mannosamine with the alcohol headgroup of PSOH through disuccinimidyl carbonate. The carbamate linkage between the carbohydrate and the lipid body provided the glycolipid in good yield while maintaining the 3, 4, and 6 hydroxyl groups of the pyranose free for accessible binding to the lectin recognition site.[11] The mannosyl group can extend approximately 7Å further into solution from the surface of the phosphatidylcholine membrane by the triethyleneglycol spacer.

PSMU was isolated as an amber colored oil with all spectral assignments matching the proposed structure.

Liposomes of PSMU with DSPC or SOPC were prepared by suspending dried films of the lipid mixtures in PBS buffer (pH 7.0), followed by extrusion through 100 nm pore polycarbonate membranes. The vesicle size range, determined by TEM imaging of the ammonium molybdate stained vesicles, was 100 – 300 nm. Lipid bilayers prepared with matrix lipids in the gel phase at room temperature (i.e., DSPC, T_g = 55 °C) or in the fluid phase at room temperature (i.e., SOPC, T_g < r.t.) allowed us to more fully assess the behavior of glycolipid organization in the presence of lectin protein.

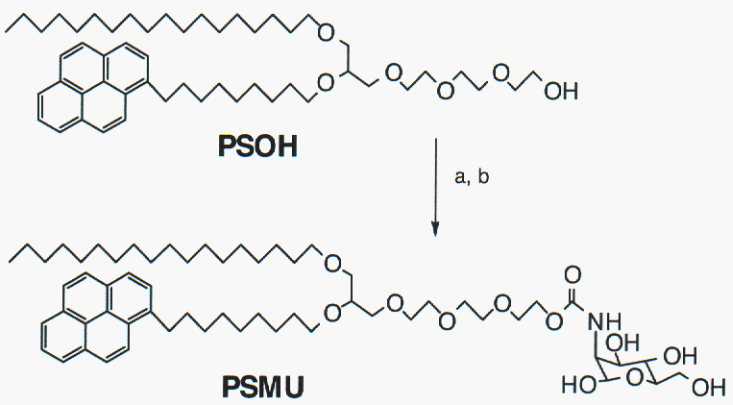

Figure 6. Synthetic preparation of mannose-functionalized, pyrene-labeled lipid PSMU. Synthetic procedures: a) disuccinylcarbamate, pyridine, DMSO, room temperature, 24h; b) mannosamine, toluene/DMF, diisopropylethylamine, room temperature, 3h.

Addition of Con A into solutions of either PSMU/DPSC or PSMU/SOPC liposomes, at a total lipid concentration of 10 μM, produces a loss in pyrene excimer fluorescence intensity with a concomitant increase in the monomer intensity. The change in fluorescence occurred relatively slowly reaching a plateau over a period of several hours for the SOPC bilayers, yet taking longer than two days for the DSPC bilayers at 25 °C. The response was distinct with the DSPC bilayers, while that for the SOPC bilayers registered only a change of ~ 10%. A series of fluorescence spectra of a stirred solution of the 5% PSMU/DSPC liposomes in the presence of 10 μM of Con A, over the period of 56 hours is shown in Figure 7. An important note from these series of spectra is the presence of an isosbestic point at 437 nm. This indicates that the fluorescence change was due to changes in the aggregational state of the pyrene moieties without contributions from fluorescence quenching mechanisms,[12] such as changes in the polarity of environment or metal ion interaction, both of which could occur if the bound protein deteriorates the lipid membrane.

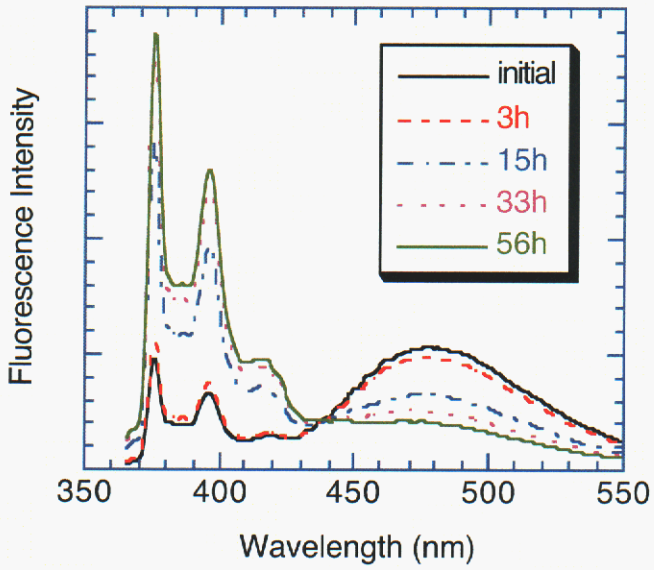

Figure 7. Fluorescence spectra of 5% PSMU/DSPC liposomes before and after exposure to 10 μM Concanavalin A in PBS buffer (pH 7.0) recorded at different time intervals.

Control experiments using non-lectin proteins and dummy ligands on the membrane surface provided further evidence of the specificity of the lectin-membrane interaction. Addition of 10 μM of bovine serum albumin (BSA) produced no significant fluorescence response from the liposomes. Likewise, by substituting for PSMU with PSOH, thus removing the carbohydrate headgroup functionality, the fluorescence response of the liposomes for Con A was completely extinguished. Binding of Con A to the PSMU containing liposomes was inhibited, albeit incompletely, using D-mannose. A two thousand-fold excess of D-mannose (10 mM) to Con A (5 μM) in solution inhibited the fluorescence response to 60% of the total uninhibited experiment. By removing the bound Con A from the membrane we would expect the original bilayer fluorescence to return, as we have seen with previous studies with metal-chelating membranes.[13,14] However, the fluorescence spectra of the Con A bound 5% PSMU/DSPC bilayers could not be reverted, even slightly, with the addition of 10 mM of D-mannose to solution indicating strong affinity of the protein for the surface.

The fluorescence results observed here appears to contradict other reports where lipid or receptor aggregation was induced by Con A binding at the membrane surface.[15,16] If one considers specific binding occurring between a protein and a glycolipid, the size mismatch is considerable. Con A is a tetramer of 26 kD proteins formed in a tetrahedral structure at pH 7.0, with the mannosyl binding site at the apex of each protein in the tetrahedron.[17] The width of the structure is

ca. 100Å. The width of a PC lipid is ca. 6 – 7Å, and the glycolipid about 50% larger. A schematic drawing of such a protein bound to the 5% glycolipid membrane depicts the contrast in size of the protein and bound glycolipid (Figure 9). It is evident from the drawing that if specific protein-glycolipid binding occurs the glycolipids will be separated either by the steric interactions of the bound proteins for one tetramer binding to one glycolipid or by the physical separation of binding sites of the tetramer binding to two or three glycolipids.

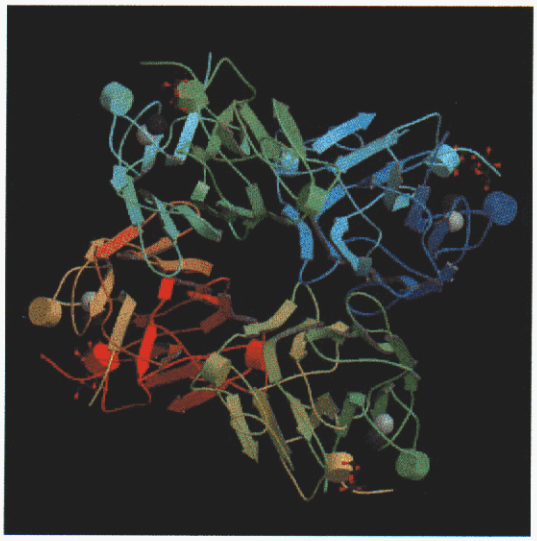

Figure 8. Crystal structure of Concanavalin A (from the Protein Data Bank).

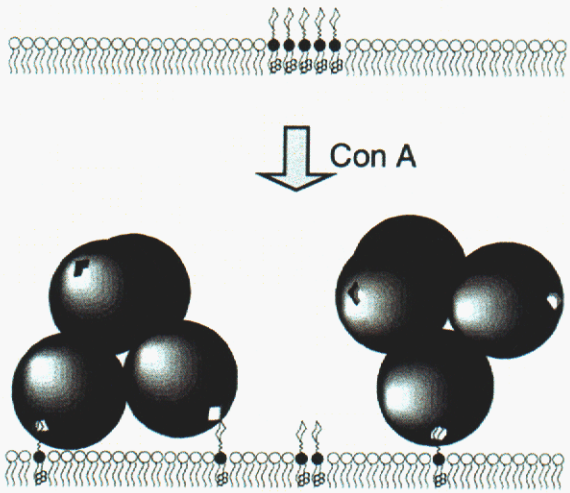

Figure 9. Schematic of PSMU/DSPC monolayer responding to Concanavalin A binding.

To further evaluate the binding interaction of Con A with this glycolipid membrane, AFM imaging of the protein bound membranes were conducted. We have previously shown that it is possible to monitor the nanoscale changes in lipid aggregation induced by chemical recognition at the membrane surface.[13,14] Using a similar route, supported lipid bilayers composed of 20% PSMU/DSPC were prepared at room temperature on a mica surface via vesicle fusion in a solution cell. Con A was then added to the solution cell at a concentration of 9 μM. Representative AFM images of the bilayer before and several hours after addition of Con A are shown in Figure 10. At the junction points of the dendritic lines were areas that appear to be high in concentration of glycolipids showing up as 60 - 90 nm wide dots or ellipsoids. The height of these areas are ~16Å, significantly taller than the 5 – 6Å heights measured on the dendrite lines, as well as taller than the modeled height difference of 10Å between PSMU and DSPC. The large height of the glycolipid regions is likely due to an effect of the dense packing of the carbohydrate headgroups. This observation with high density receptor regions is not unique and has been also observed in some instances with our metal chelating lipid membranes.[18] Our claim that the lightest shaded areas belong to aggregates of PSMU is further corroborated by the measurement of the overall area occupied by the lines and dots amounting to approximately 20% of the total membrane area.

Several hours of incubation with Con A produces the right side image of Figure 10. An increase in noise and loss of resolution was always observed after the addition of Con A suggesting that the protein interferes with, and possibly adsorbs onto, the AFM tip. The lightest shaded features were consistently observed over multiple experiments following the addition of Con A and thus we distinguish them as the protein bound to the membrane surface. Individual structures of circular shape and near similar size as the Con A tetrameric structure can be found sporadically covering the surface. The measured diameter of the structure, which is 22 nm full width at half maximum, is comparable to the 10 nm width of Con A considering image convolution from the AFM tip.[19] Two of these Con A structures are indicated by arrows in Figure 9B. The height of these individual structures only measures about 10 – 20Å, considerably shorter than their known width, whereas large aggregates in the same image yield heights of ca. 50Å. While the heights of the individual proteins, which approach the resolution limit of the AFM on lipid membranes, may be difficult to assess the general observation of bound protein heights measuring 50Å or less suggest that Con A does not exist as a tetramer atop the membrane surface. Rather, it either inserts into the membrane or, alternatively, denatures or forms dimers against the membrane. AFM imaging alone cannot make this distinction.

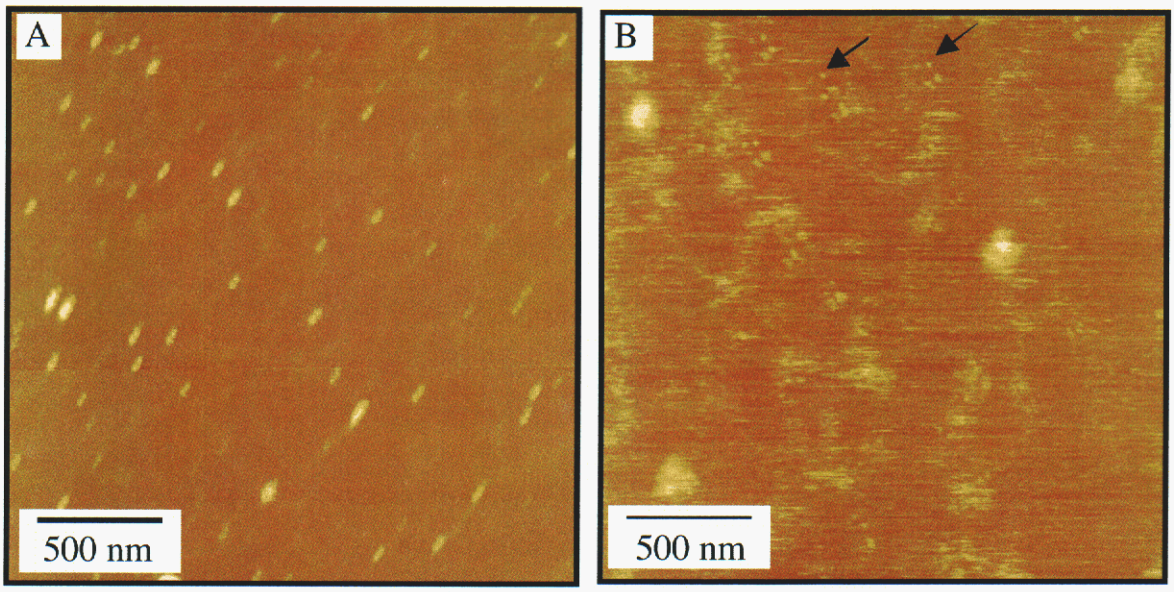

Figure 10. AFM images of the 20% PSMU/DSPC membrane (A) before and (B) after six hours of exposure time with 9μM Con A in PBS buffer (pH 7.0) at room temperature. Arrows indicate structures that of possible individual Con A tetramers. (Height scale = 5 nm).

The ability to monitor molecular associations both optically and with nanoscale resolution provides a level of detail that is necessary to fully characterize protein-membrane interactions. Our pyrene-labeled glycolipid PSMU allows one to evaluate the effect of specific protein interactions upon lipid associations within the membrane. Concanavalin A binding with the mannosyl headgroup of PSMU induced a dispersion of the glycolipid evidenced by both fluorescence and AFM monitoring of the system. Steric interactions between the protein-lipid complexes formed at the membrane and the physical separation of binding sites within the tetrameric structure are the likely reasons for the observed dispersion of initially aggregated glycolipid. Protein insertion into the membrane also appears to take place further complicating the interactions of these dynamic materials. The binding of protein and the lipid reorganization of the membrane are slow, proceeding on the order of days. These studies suggest that membrane-protein associations are complex incorporating various phenomena, such as steric crowding, molecular mobility, and protein insertion. These issues are indeed difficult to measure and monitor but are important for understanding the basic principals of cell membrane biology.

Polydiacetylene/silica sol-gel material

Here we report the self-assembly of conjugated polymer/silica nanocomposite films with hexagonal, cubic, or lamellar mesoscopic order using polymerizable amphiphilic diacetylene molecules as both structure-directing agents and monomers. The self-assembly procedure is rapid and incorporates the organic monomers uniformly within a highly ordered, inorganic environment.

Polymerization results in polydiacetylene (PDA)/silica nanocomposites that are optically transparent and mechanically robust. Compared to the corresponding ordered, diacetylene-containing films prepared as Langmuir monolayers[20] or by Langmuir-Blodgett[20] deposition the nanostructured inorganic host alters the diacetylene polymerization behavior, and the resulting nanocomposite exhibits unique thermo-, mechano-, and solvato-chromic properties. We believe self-assembly to be an efficient, general approach to the formation of conjugated polymer/inorganic nanocomposites, wherein the inorganic framework serves to protect, stabilize, and orient the polymer, mediate its performance, and provide sufficient mechanical integrity to enable integration into devices and microsystems.

Our approach to conjugated polymer/silica nanocomposites employs a series of oligoethylene glycol functionalized diacetylenic ($PCEG_n$) surfactants (where n = 3,4,5, or 10, prepared by coupling ethylene glycols with the acid chloride of 10,12-pentacosadiynoic acid) both as amphiphiles to direct the self-assembly of thin film silica mesophases[21] and as monomeric precursors of the conjugated polymer, PDA. Beginning with a homogeneous solution of silicic acid and surfactant prepared in a tetrahydrofuran (THF)/water solvent with initial surfactant concentration c_o much less than the critical surfactant micelle concentration *cmc*, we use evaporative dip-coating, spin-coating, or casting procedures to prepare thin films on silicon <100> or fused silica substrates. During deposition, preferential evaporation of THF concentrates the depositing film in water and nonvolatile silica and surfactant species. The progressively increasing surfactant concentration drives self-assembly of diacteylene/silica surfactant micelles and their further organization into ordered, 3-dimensional, liquid crystalline mesophases. Ultraviolet (UV) light-initiated polymerization of the DA units, accompanied by catalyst-promoted siloxane condensation, topochemically convert the colorless mesophase into the blue PDA/silica nanocomposite, preserving the highly ordered, self-assembled architecture.

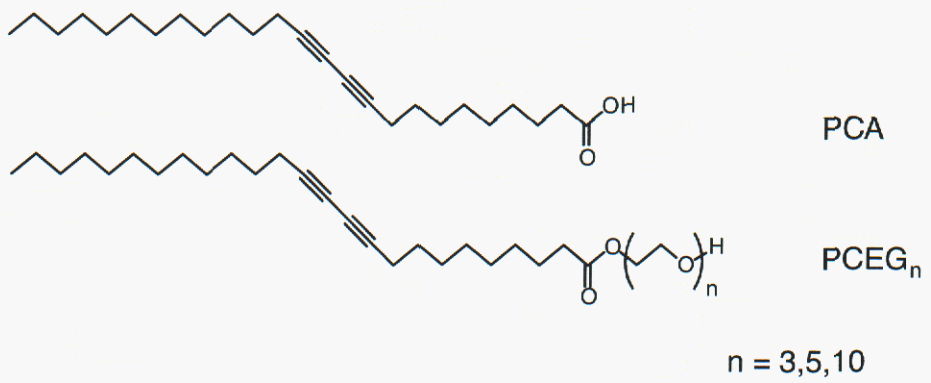

Figure 11. Molecular structures of polydiacetylene surfactants: PCA – 10,12-pentacosadiynoic acid, $PCEG_n$ – oligoethylene glycol 10,12-pentacosadiynoic acid esters.

Figure 12 shows a patterned blue PDA/silica nanocomposite film, with a hexagonal mesostructure (prepared using **1**, with n=5), formed by UV exposure through a mask and the corresponding patterned red film formed subsequently by heating to 100°C. The TEM image and X-ray diffraction (XRD) spectrum of the material is shown in Figure 13. Whereas lamellar mesophases (prepared using **1** with n=3) show qualitatively similar behavior, cubic mesostructures (prepared using **1**, with n=10) and Langmuir monolayers and trilayers (prepared using neat **1** with n=3,5,or 10) remain colorless upon UV exposure and during heating. The different behaviors of lamellar and Langmuir films emphasize the importance of the nanostructured inorganic host on PDA polymerization. In both systems the diacetylenic surfactants are organized into highly oriented planar configurations with the EO headgroups disposed toward the hydrophilic interface, either water (Langmuir films) or polysilicic acid (nanocomposites). Despite these similar organizations, we postulate that Langmuir films do not polymerize because the reactive DA moieties are spaced too far apart as indicated by the molecular areas measured at 30 mN/m in a Langmuir trough: DA-EO_1=24Å^2, DA-EO_3 = 38Å^2, DA-EO_5 = 46Å^2. Closer spacing of the oligoethylene glycol headgroups (and correspondingly the diacetylenic moieties) within the self-assembled nanocomposites (lamellar, hexagonal, or cubic) is anticipated from the requirement for charge density matching at the R-EO_{m-y}[EO·H_3O^+]y··yX^-··w$I^{\delta+}$ interface (where R = alkyl chain, X = Cl^-, and $I^{\delta+}$ = the partial charge of the silica framework) that reduces the optimal EO headgroup area a_o.

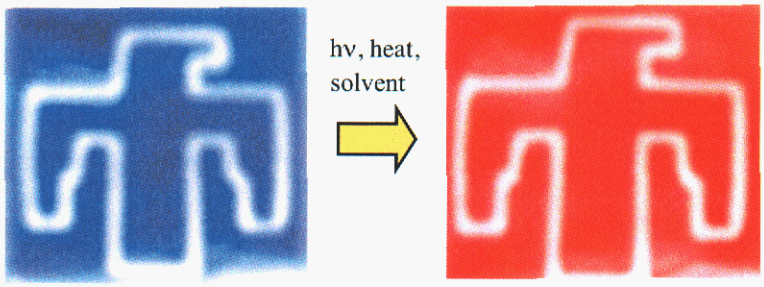

Figure 12. Colorimetric change of PCEG/silica sol-gel material.

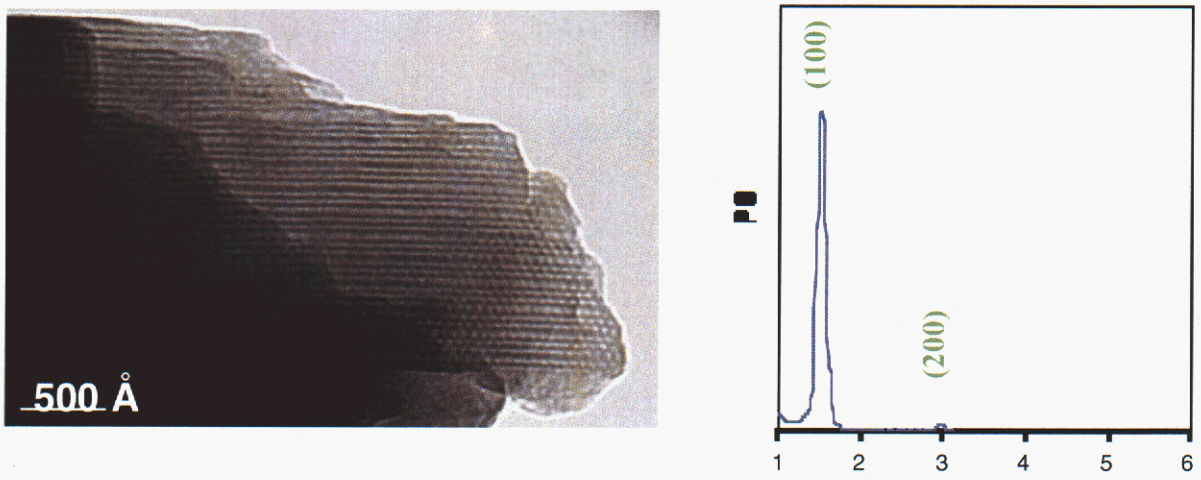

Figure 13. TEM image (left) and XRD spectrum of 8% $PCEG_5$/silica sol-gel thin film.

The use of polymerizable surfactants as both structure directing agents and monomers in the various evaporation-driven self-assembly schemes developed recently represents a general, efficient route to the formation of robust and functional nanocomposites.

Silica sol-gel/lipid bilayer composite material

We found that spherical, bilayer lipid aggregates, or liposomes, can be successfully immobilized using an aqueous sol-gel procedure. The structure of liposomes, composed of biological or bio-mimetic lipids, is fairly robust under aqueous conditions and ambient temperatures but can easily degrade in the presence of organic solvents and high temperatures. The sol-gel process provides a facile method of immobilizing molecular aggregates with no detectable structure modification. To demonstrate the generality of this immobilization technique for liposomes we looked at non-polymerized and polymerized lipid systems. For the non-polymer lipid aggregate system we used the heavy metal sensitive PSIDA/DSPC fluorescent liposome. Lipid mixtures of 5% PSIDA in DSPC were prepared as small unilamellar vesicles (SUV) with mean diameter of 49 nm (59 nm distribution width)[22] determined by dynamic light scattering.

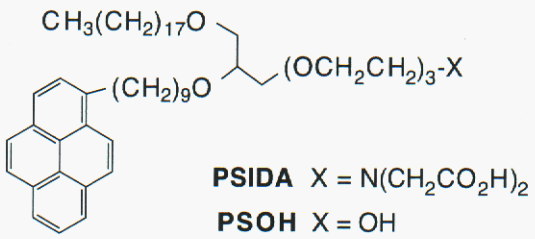

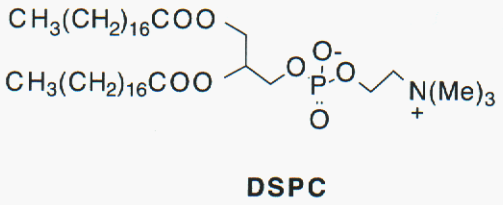

DSPC

Figure 14. Molecular structures of PSIDA and DSPC.

During sol-gel processing we conducted fluorescence studies of the materials to examine if the TMOS oligomers and generated methanol would have any influence over the structural properties of the lipid bilayer. The data indicate that the lipid bilayers prepared with 5% PSIDA/DSPC liposomes are maintained with minimal structural changes from new to aged gels. Excitation of the sol-gel material at 346 nm yields emission maxima at 375 nm for the monomer and at 470 nm from excimer formation of the pyrene fluorophores on the PSIDA lipid tail. The excimer formation at these lipid concentrations (6×10^{-6} M) can only occur if the lipids are in an aggregated state. Freely suspended 5% PSIDA/DSPC liposomes in MOPS buffer solution show identical spectral character to the entrapped liposomes. Had the liposome been disrupted by the sol-gel process resulting in dissolved lipids in solution, the PSIDA lipid would yield only pyrene monomer emission. In studies looking at the effect of methanol on the lipid aggregate structure significant changes in fluorescence intensity and excimer to monomer intensity ratios (E/M) were observed at concentrations above 10% methanol/water. The minimal fluorescence changes observed for the entrapped liposomes suggest that the generated methanol from sol-gel processing is lower than 10%.

The fluorescence response of the liposome/sol-gel material to divalent metal ions can be observed visually for the detection of some metals (e.g., Cu^{2+}, Co^{2+}) down to micromolar concentration with the green pyrene excimer emission yielding to the bluish emission of the monomer. Equilibration to metal ion is typically reached within 24 hours. Figure 15 shows the silica sol-gel immobilized 5% PSIDA/DSPC lipid bilayer composite material before and after exposure to Cu(II) ion (10 μM), displaying the responsiveness of the bilayers to their target analyte and the permeability of the silica matrix to the analytes.

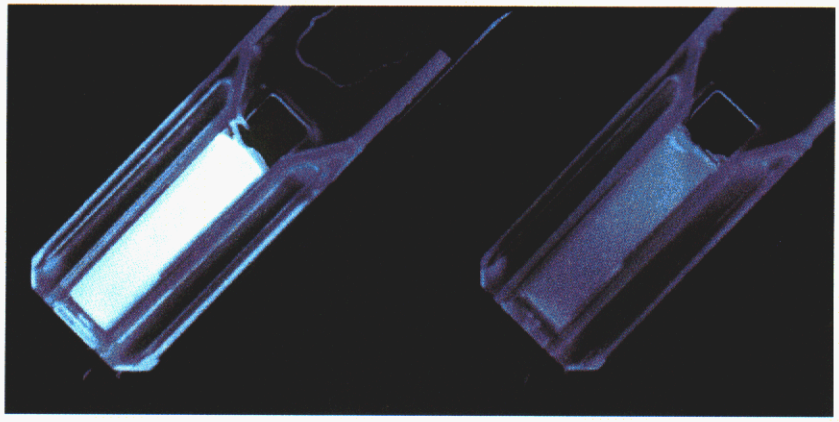

Figure 15. Picture of 5% PSIDA/DSPC bilayers in silica sol-gel matrix before (left) and after (right) exposure (12 hours) to 10 μM $CuCl_2$ in phosphate buffer at pH 7.4.

For sensor applications, we also addressed the response time and recycling properties of the liposome/sol-gel composite. For the heavy metal sensor, we used the 5 mm thick gel monoliths for our studies. The monoliths show response times for complete equilibration, in a stirred solution, ranging from hours with tens of micromolar Cu^{2+} concentrations to days with sub-micromolar concentrations. An observable color change from green to blue with metal ion presence begins at the edges of the monolith and grows inward until the color change is homogeneous throughout. Addition of ethylenediamine tetraacetic acid (EDTA) solution (10 μM) recovers the metal sensor within several hours. The Cu^{2+}-EDTA cycle can be conducted several times without any loss of sensor performance.

Microoptical waveguide platform

We directed fabrication efforts toward realizing a reusable optical platform to demonstrate and characterize the optical beam/functionalized film interaction. We required the optical substrate to have one smooth surface where a functionalized film could be applied with a Langmuir-Blodgett or dip-coat application. After the film interaction is characterized, the film can be removed and another applied. We implemented a low-profile, reflective grating on the transparent optical platform's other surface to direct the light, through substrate mode propagation, to discrete interaction spots down the length of the platform as shown in Figure 16. An optical beam/functionalized film interaction, such as fluorescence, will be directly observable or may be quantified with a scanned Si detector.

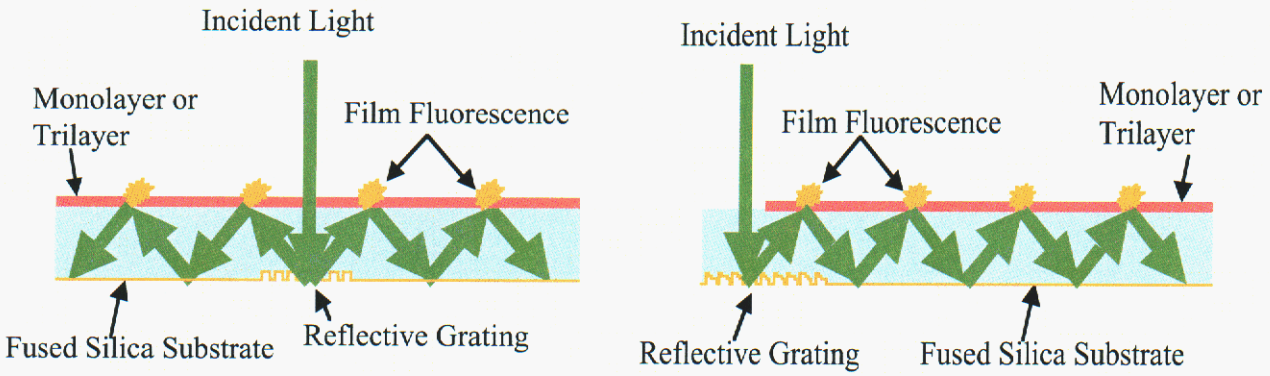

Figure 16. Optical coupling configurations for two- (left) and four- (right) level gratings.

Predicted diffraction efficiencies are shown for a two-level (Figures 17) and four-level (Figures 18) grating. A two-level grating design symmetrically reflects light at both +/- 45 degrees, each with an efficiency of approximately 45%. A four-level reflective grating asymmetrically directs most of the light into a desired direction.

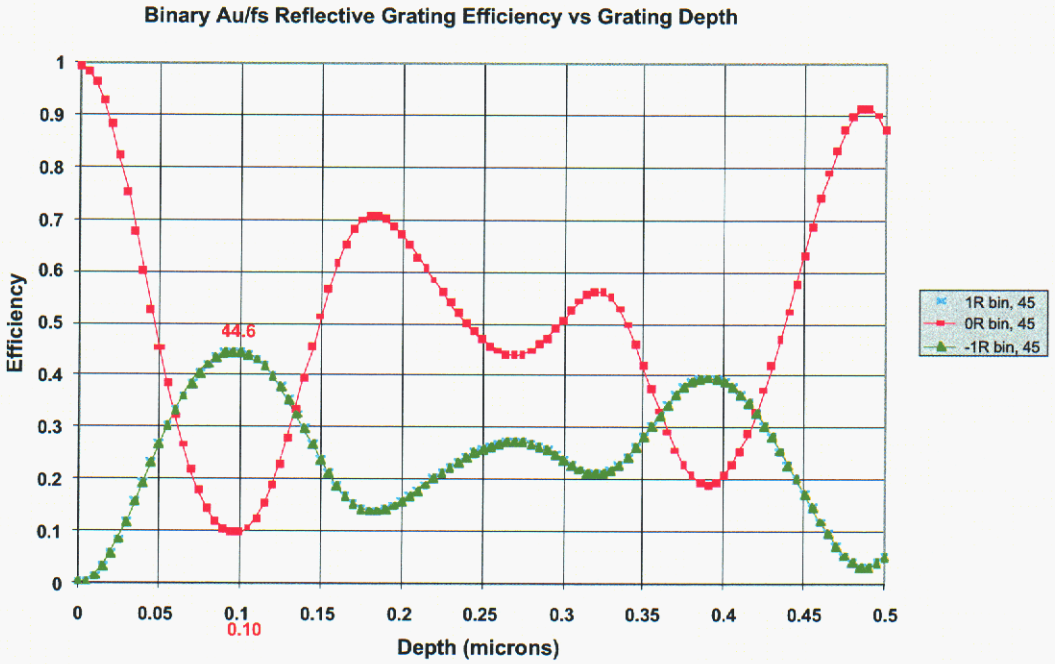

Figure 17. Predicted diffraction efficiency from Rigorous Coupled Wave Analysis for a two-level grating.

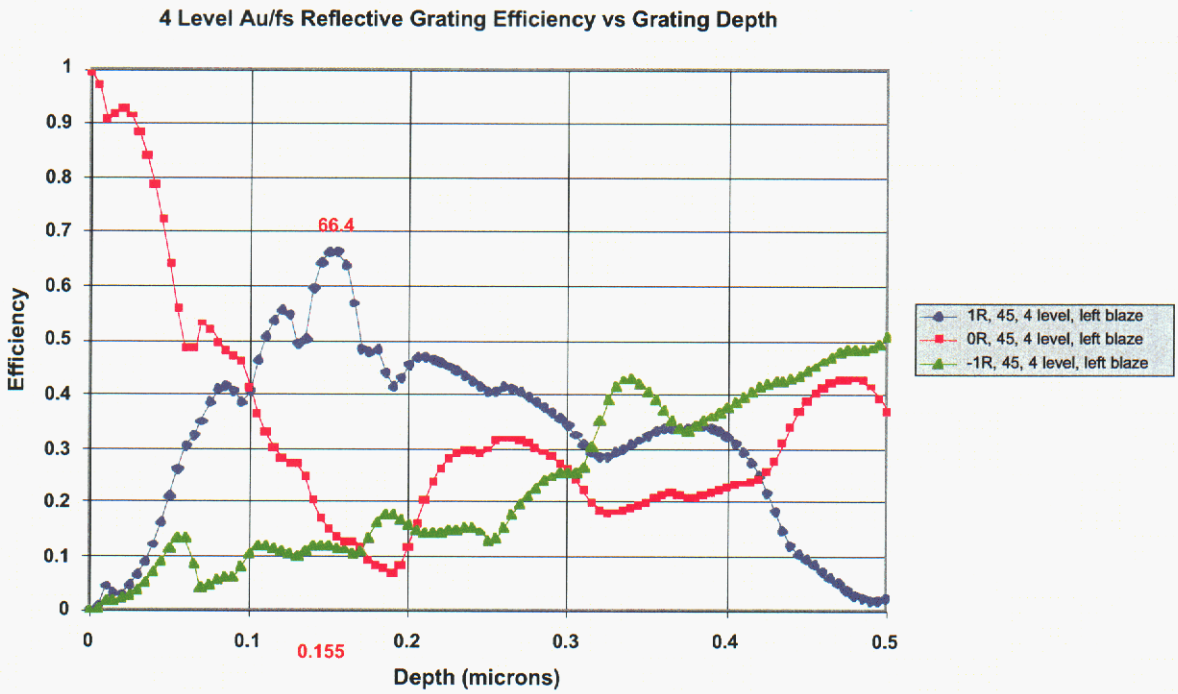

Figure 18. Predicted diffraction efficiency from Rigorous Coupled Wave Analysis for a four-level grating.

The two-level grating has a minimum feature size of 0.26 μm. The four-level grating design is more aggressive in that it contains smaller feature sizes and requires two mask write and etch fabrication cycles. In fact, several technical challenges were expected for the four-level grating design: 1) realizing extremely small grating feature sizes (0.087 μm) due to the low 0.532 μm design wavelength and the 4-level design, 2) aligning the second mask relative to the fine features of the first mask, 3) conformally coating the high-aspect ratio grating features with a relatively thick gold layer, and 4) obtaining precise etch depths for optimal reflection efficiency.
We mitigated the first challenge by initially scaling this 4-level design to an input wavelength of 0.85 μm, where the smallest feature is now 0.138 μm. In this regime we successfully met challenges 1) and 2). However, efficiency measurements indicated that challenges 3) and 4) were only partially met.

Although four-level gratings are predicted to produce higher efficiency diffracted beams, there was concern that the high-aspect ratio, small pitch fused silica features were breaking off and re-depositing across the grating, either during processing or characterization. With this in mind, we fabricated the two-level gratings configurations in the second-generation optical platform layout. We addressed issues with conformal Au coating by moving Au deposition to a planetary motion stage, ensuring Au deposition on the grating vertical grating walls as well as the horizontal mesas. Some low efficiency results were traced to mask residue that remained upon the grating after

cleaning cycles. The masking and clean processes were modified to erase any detrimental debris, as shown in Figure 19.

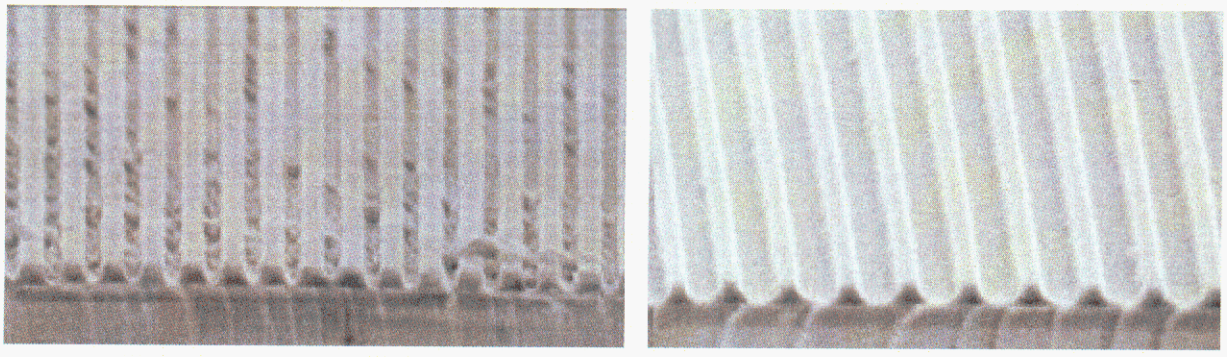

Figure 19. Scanning electron microscope pictures of a two-level grating with detrimental mask residue (left) and after modified cleaning process to remove debris (right).

Integrated Structure

Transparent silica sol-gel materials incorporating the above mentioned optically responsive self-assembled structures should offer excellent physical properties to coat the microoptical structure, protect the self-assembled, organic materials, and permit light propagation for proper device operation. Our first attempt at the preparation of the integrated structure was a thin film, dip-coated polydiacetylene/silica material on a two-level microoptical platform.

An optical platform utilizing a two-level, gold-coated diffraction grating was fabricated in fused silica. This platform was first coated with a 200 – 300 μm thick polydimethylsiloxane (PDMS) film on the gold-coated side by spin casting. The PDMS film acted as a sealant to protect the gold pads and etched features in the fused silica from the sol-gel coating. After the PDMS film was cured a 2 μm thick PCEG5/silica sol-gel was deposited over the entire fused silica slide by dip-coating. The sol-gel composition was the same as that reported in the *Polydiacetylene/silica sol-gel material* section above and in reference 21. The colorless film was then either transformed into blue- or red-phase polydiacetylene via UV light polymerization.

The optical material/microoptical device integrated structure was then qualitatively characterized to determine the efficiency of light propagation through the sensor material and the optical yield of the material. The integrated structure, with a red-phase polydiacetylene/silica material, was mounted on a holder and illuminated with a 548 nm laser aimed at the diffraction grating. In Figure 20, it is possible to see the green laser light as it propagates through the fused silica with several reflections off the gold stripe on the side opposite of the incident laser beam. In the dark the laser light was equally visible as it reflects down the device, although the exposure rate of the digital camera did not capture reflection spots with weaker intensities. Using a 560 nm cutoff

filter it was possible to observe the orange-red fluorescence of the red-phase polydiacetylene several reflections down the device. In Figure 20, again only the fluorescence from the first reflection point was observable.

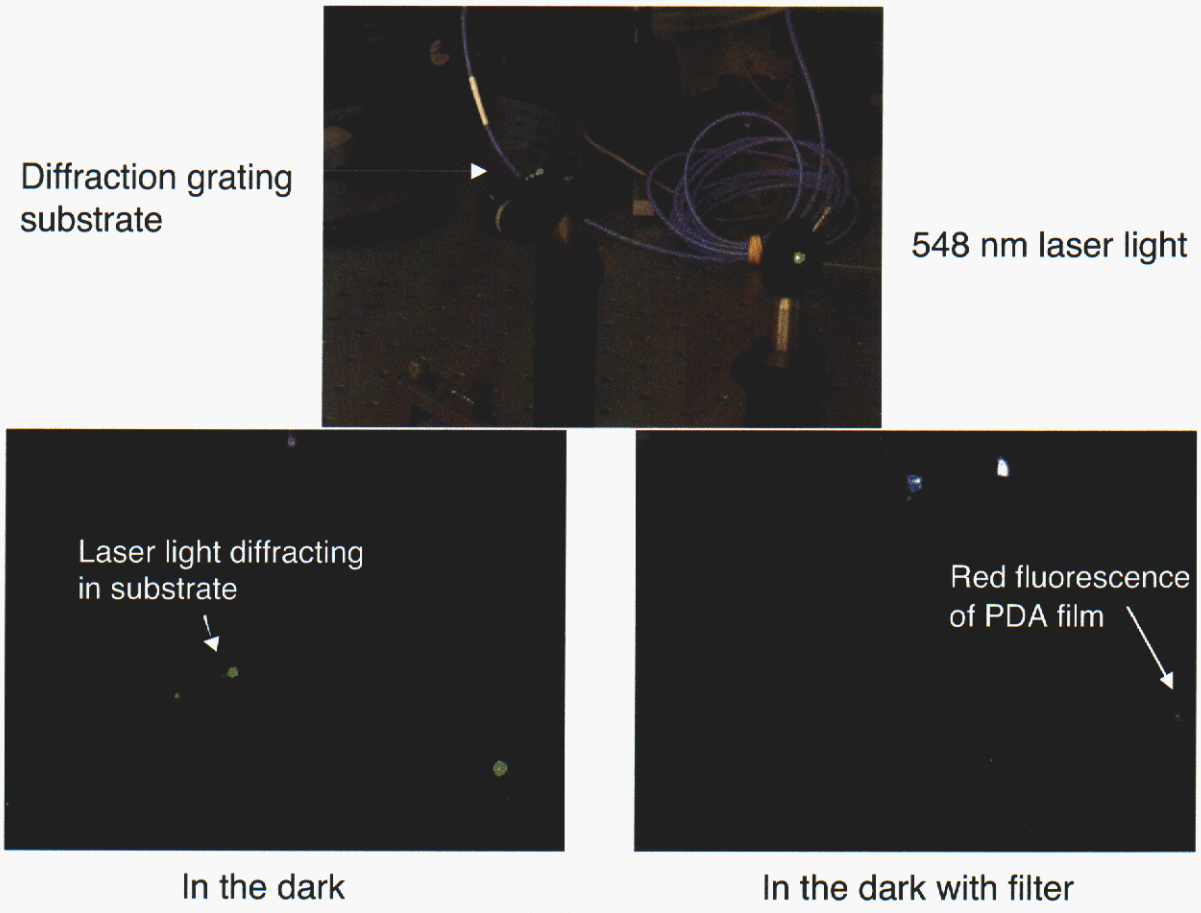

Figure 20. Pictures of optical response of the integrated structure consisting of a PDA/silica sol-gel film on the microfabricated optical device. The integrated device is shown above with a 548 nm laser light illuminating the grating to yield several reflections of green light down the device structure. Below are pictures of the same set up in the dark (left) and with a 560 nm cutoff filter (right) to observe the orange-red fluorescence of the PDA material.

Conclusions

In this project we have developed a number of novel optical sensor materials and microoptical systems, and coupled them to form an integrated device. We report on a few of the developed self-assembling, optical sensor materials that exhibit high selectivity for metal ions, proteins, and temperature. A pyrene-labeled lipid bilayer, functionalized with 18-crown-6 functional groups, exhibited high selectivity for lead and mercuric ions producing a fluorescence response that is a product of a membrane rearrangement resulting from the chemical recognition event between the crown ether and the metal ions. Similarly, a mannose-functionalized membrane selectively bound the lectin protein Concanavalin A producing a readily monitored fluorescence response. In both systems the structural changes that occur in the material due to host-guest interaction were probed at the nanoscale using *in situ* AFM imaging. Hierarchical polydiacetylene/silica structures were also produced through the micellar forming properties of oligoethylene glycol functionalized diacetylene amphiphiles. The materials could be readily converted to polymers via UV irradiation creating the blue or red colors characteristic of polydiacetylene. Upon heating the materials or exposure to solvent vapors the materials could be converted from blue to red. This material was coupled to a microfabricated optical structure to form an integrated device. The microoptical device was designed and created with two- and four-level gratings that propagated light down the fused silica structure via reflections off the opposing surfaces. The light coming off the surface at the reflection points provided a number of illumination sources for the nanocomposite materials in an array format. Optical probing of the integrated device composed of the polydiacetylene/silica sol-gel with the two-level grating structure demonstrated the concept.

References

1) Izatt, R. M.; Pawlak, K.; Bradshaw, J. S.; Bruening, R. L. *Chem. Rev.* **1991**, *91*, 1721 - 2085.

2a) Luca, C.; Azab, H. A.; Tanase, I. *Anal. Lett.* **1985**, *18*, 449 - 465. b) Buschmann, H.-J. *Inorg. Chim. Acta* **1985**, *98*, 43 - 46. c) Chen, L.; Bos, M.; Grootenhuis, P. D. J.; Christenhusz, A.; Hoogendam, E.; Reinhoudt, D. N.;van der Linden, W. E. *Anal. Chim. Acta* **1987**, *201*, 117 - 125. d) Hayashita, T.; Sawano, H.; Higuchi, T.; Indo, M.; Hiratani, K.; Zhang, Z.-Y.; Bartsch, R. A. *Anal. Chem.* **1999**, *71*, 791 - 795.

3) Ng, K.; Pack, D. W.; Sasaki, D. Y.; Arnold, F. H. *Langmuir* **1995**, *11*, 4048 - 4055.

4) Sasaki, D. Y.; Padilla, B. E. *Chem. Comm.* **1998**, 1581 - 1582.

5) Sasaki, D. Y.; Waggoner, T. A. *Proc. SPIE-Int. Soc. Opt. Eng.* **1999**, *3606*, 46 - 54.

6) Sasaki, D. Y.; Shnek, D. R.; Pack, D. W.; Arnold, F. H. *Angew. Chem., Int. Ed. Engl.* **1995**, *34*, 905 - 907.

7) The fluorescence response of the 20% PS18C6/DSPC liposomes was generally the same as the 5% loaded bilayers, but with a larger initial E/M ratio. The selectivity for Pb2+ is identical between the bilayer materials, but the E/M response was slightly stronger for the 20% bilayer compared to the 5% bilayer.

8) See Figure S6 in the Supporting Information.

9a) Song, X.; Nolan, J.; Swanson, B. I. *J. Am. Chem. Soc.* **1998**, *120*, 11514 - 11515. b) Song, X.; Nolan, J.; Swanson, B. I. *J. Am. Chem. Soc.* **1998**, *120*, 4873 - 4874.

10a) Kreis, T.; Vale, R. *Guidebook to the Extracellular Matrix, Anchor, and Adhesion Proteins*; 2nd ed.; Kreis, T.; Vale, R., Ed.; Oxford University Press: New York, 1999. b) Bog-Hansen, T. C.; Freed, D. L. J., Ed. *Lectins: Biology, Biochemistry, Clinical Biochemistry*; Sigma: St. Louis, 1988; Vol. 6, pp 757.

11) Hardman, K. D.; Goldstein, I. J. *The Structure and Activity of Concanavalin A*; Atassi, M. Z., Ed.; Plenum: New York, 1977; Vol. 2, pp 373 - 416.

12) Kinnunen, P. K. J.; Koiv, A.; Mustonen, P. *Pyrene-Labelled Lipids as Fluorescent Probes in Studies on Biomembranes and Membrane Models*; Wolfbeis, O. S., Ed.; Springer-Verlag: New York, 1993, pp 159.

13) Sasaki, D. Y.; Waggoner, T. A.; Last, J. A.; Alam, T. M. *Langmuir* **2002**, *18*, 3714 - 3721.

14) Last, J. A.; Waggoner, T. A.; Sasaki, D. Y. *Biophy. J.* **2001**, *81*, 2737 - 2742.

15) Ketis, N. V.; Grant, C. W. M. *Biochim. Biophys. Acta* **1983**, *730*, 359 - 368.

16) Kitano, H.; Ishino, Y.; Yabe, K. *Langmuir* **2001**, *17*, 2312 - 2316.

17a) Moothoo, D. N.; Canaan, B.; Field, R. A.; Naismith, J. H. *Concanavalin A Structure 1BXH,* Protein Data Bank, http://www.rcsb.org/pdb/. b) Kalb, A. J.; Habash, J.; Hunter, N. S.; Price, H. J.; Raferty, J.; Helliwell, J. R. *Met. Ions Biol. Syst.* **2000**, *37*, 279 - 304.

18) Unpublished results.

19) Warner, M. J.; Gilchrist, M.; Schindler, M.; Dantus, M. J. Phys. Chem. B **1998**, *102*, 1649 – 1657.

20) Sasaki, D. Y.; Carpick, R. W.; Burns, A. R. *J. Coll. Interface Sci.* **2000**, *229*, 490.

21) Lu, Y. F. et al. Nature 1997, 389, 364 – 368.

22) Shnek, D. R.; Pack, D. W.; Sasaki, D. Y.; Arnold, F. H. *Langmuir* **1994**, *10*, 2382.

DISTRIBUTION:

10	MS	1413	D. Sasaki
1		0603	S. Kemme
1		0603	J. Wendt
1		0603	T. Carter
1		0603	S. Samora
1		1202	M. Warren
2		1349	C. J. Brinker
1		1411	M. Sinclair
1		1413	J. Last
1		1413	B. Bondurant
1		1413	T. Waggoner
1		1413	P. Dressendorfer
1		1413	T. Michalske
1		0188	C. E. Meyers, LDRD Office
1		9018	Central Technical Files, 8945-1
2		0899	Technical Library, 9616
1		0612	Review & Approval Desk, 0612
			For DOE/OSTI